A Low Power-consumption and Transient Nonvolatile Memory Based on Highly Dense All-Inorganic Perovskite Films

Ghulam Abbas, Muhammad Hassan, Qasim Khan, Haifei Wang, Guigang Zhou, Muhammad Zubair, Xiuru Xu,* and Zhengchun Peng*

Inorganic perovskite-based memory devices have attracted tremendous attention due to their higher level of stability, more feasible synthesis conditions and better performance, as compared to organic–inorganic hybrid perovskite-based devices. However, better film morphology is an essential issue for the performance of these devices. Here, the all-inorganic halide perovskite cesium lead bromide ($CsPbBr_3$) films are successfully fabricated via a unique solution processable deposition method at ambient conditions. These films possess satisfactory surface morphology with high crystallinity. These are utilized for reproducible resistive switching layers in the gold/$CsPbBr_3$/indium tin oxide/Glass memory applications. A series of resistive switching layers (i.e., $CsPbBr_3$) with varied thicknesses in the range of 200–500 nm are precisely tailored. The resistive switching responses and retention properties of $CsPbBr_3$ based-memory devices exhibit long-term retention (exceeding 10000 s), high on/off ratio (up to 10000), low power consumption (set voltage at 0.25V), and good reproducibility. A model for the formation of filaments in the $CsPbBr_3$ layer is proposed to describe the resistive switching mechanism. Furthermore, the devices exhibit excellent transient behavior, which is beneficial for the security of data storage. These characteristics reveal that cesium lead halide based memristor is promising to be utilized as the next-generation smart memory device.

1. Introduction

The rapidly growing interest in highly efficient and reliable memory devices for the next-generation digital communications demands remarkable attention for new approaches toward storage devices.[1] Resistive switching random access memory devices (RRAM) have been prominently contemplated to fulfill the future demands of nonvolatile memory devices, because of their minimum power consumption,[2] ultrahigh efficiency, multibit data processing ability, fast switching speed, and

long-term data retention.[3] Both volatile and nonvolatile memories based on perovskites, oxides and 2D layered semiconductors are getting more and more attention in everyday computing systems to reach the acute favorable trade-off between efficiency and cost.[4] Due to different etiquettes for "storage" and "memory," the data storage devices can be classified into two main types. One type is the memristors, which are adjacent to the processer core and required to be fastest in operation, making them expensive because of their largest chip area. The other type is the main memory, which is usually on the separated chip with low operating speed and relatively lower cost. Moreover, memory devices have been also reported as a promising candidate to perform neuromorphic function implementation. For example, by tuning the external electrical stimuli to emulate common nociceptive behaviors and neuropathic pain in damaged tissue.[5]

Currently, a large number of reports have been published on organic–inorganic hybrid perovskites, owing to their remarkable performances with superior optoelectronic properties including higher light absorption coefficients, high dielectric constant, better electrons/holes mobility and long-range ambipolar charge transport over other materials.[6] However, the presence of organic cations in hybrid perovskites makes them weak against thermal and air resistance. To improve the stability of perovskites, the unstable organic part is replaced by inorganic cesium (Cs) ions to form air stable inorganic halide perovskite ($CsPbX_3$). Inorganic halide perovskite with general formula $CsPbX_3$, where X represents halide ions either chlorine (Cl-), bromine (Br-), or iodine (I-) is widely used in many optoelectronic devices including high efficiency solar cells, self-powered photodetectors, waveguides, improved quantum efficiency light-emitting diodes, lasing and bioimaging.[7–10] Researchers are working to fabricate highly dense and uniform inorganic perovskite films with minimum roughness and better film morphology for high performance optoelectronic applications. There are several reports in which researchers reported improved surface morphology and better efficiencies of devices.[11] Moreover, lots of efforts are still required to make them feasible for practical applications in terms of improved

G. Abbas, M. Hassan, Q. Khan, H. Wang, G. Zhou, M. Zubair, X. Xu, Z. Peng
Center of Stretchable Electronics and NanoSensors
College of Physics and Optoelectronic Engineering
Shenzhen University
Shenzhen 518060, China
E-mail: xiuruxu@szu.edu.cn; zcpeng@szu.edu.cn

surface morphology, minimum pinholes, less defects, and better responses. In this study, we used CsPbBr$_3$ inorganic perovskite materials for memory applications considering their better stability as compared to CsPbI$_3$ which degrades quickly to nonperovskite phase at room temperature. The general device structure for ReRAM is top electrode metal/switching layer/bottom (MSM) electrode metal structure where sandwiched switching insulator layer works as storage media.[12] External bias voltage initiates the resistive switching of RRAM from high resistance state (HRS) to low resistance state (LRS) by forming conductive filaments. Previously reported resistive switching phenomenon includes, threshold, unipolar, bipolar, and complementary, etc.[13,14] These mechanisms can be explained with the help of trap charge densities, Pool–Frenkel emission, space charge limited current (SCLC), Schottky barrier, alignments of conductive filaments (CFs), and Fowler–Nordheim (FN) tunneling.[15] Recently, Han and coworkers reported the metal conductive filaments formation and inhalation effect from CsPbBr$_3$ quantum dot based resistive switching devices. External electric field and light irradiation can trigger the set and reset states of the device, with remarkable resistive switching effects.[16] For MSM sandwich structure, electrodes are investigated by considering different metallic materials and the sandwiched switching layer is usually composed of metal oxides, either insulating oxides, or complex oxides (SrTiO$_3$ and BaTiO$_3$).[17] High-temperature synthesis, large forming voltage and low reproducibility are the main drawbacks of oxide-based RRAMs. The breakthrough for RRAMs by utilizing novel functional materials are highly desirable for less energy consumption and long-term stabilities.

Gu and coworkers initiated new research on hybrid organic–inorganic perovskite material as memristor by successful fabrication of devices with relative efficiency, which provided a path toward a new family of perovskite materials.[18] Then, organic cations present in hybrid organic–inorganic perovskite are the main hurdle for their future development due to thermal instability. To resolve the thermal stability issue, organic cations can be replaced by inorganic cations (Cs). Recently, cesium/cesium hybrid perovskite memory devices, light-emitting diodes,[19] and solar cells[20] with maximum efficiency and possessing long term stability under extreme environmental conditions are widely been reported.[21] It has been reported that the entirety of inorganic perovskites based on Cs cations are thermally and structurally more stable than hybrid perovskites under 100 °C or even higher temperature.[22] All-inorganic perovskites are remarkable competitors toward efficient and stable memory devices for high scalability, less power consumption and maximum operating speed using ambient and low-cost fabrication processes.[23]

In this work, all-inorganic perovskite CsPbBr$_3$ was fabricated as the active layer for memory operations. The active layer was successfully deposited on a precisely washed indium tin oxide (ITO)-coated glass substrate by a solution processable two-step spin coating method. Reproducible and reliable nonvolatile memory response was observed. Current voltage measurements were carried out to demonstrate the electrical reliability. This work offers a better understanding as well as utilization of entirely inorganic perovskite for stable, highly efficient, and reproducible next-generation resistive switching devices.

2. Results and Discussion

We have successfully prepared CsPbBr$_3$ based multiple memory cells by a two-step spin coating method at room temperature under ambient conditions. The thickness of the storage media (the perovskite layer) can be controlled by varying synthesis conditions. We successfully deposited the thicknesses with a range of 200–500 nm. The device structural diagram for the top electrode gold (Au)/switching layer CsPbBr$_3$/bottom electrode ITO/glass memory structure is presented in **Figure 1**a with CsPbBr$_3$ crystal structure shown as Figure 1a. Figure 1b represents the
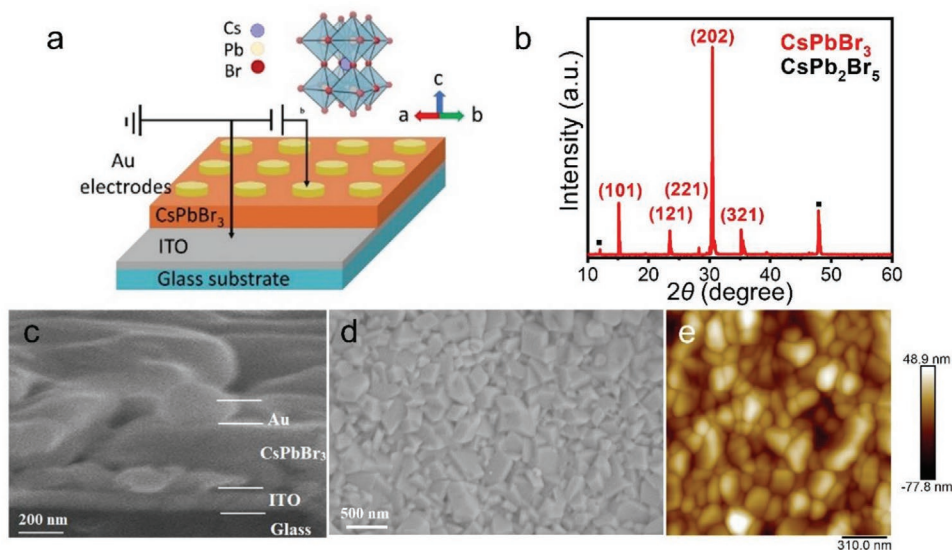

Figure 1. a) The illustration of the device structure with the CsPbBr$_3$ crystal structure. b) XRD patterns of the CsPbBr$_3$ thin film with CsPb$_2$Br$_5$ peaks (marked by black dots). c) The cross-sectional SEM image of the memory device. d) The top view of SEM and e) AFM topography images of the CsPbBr$_3$ thin film.

**ADVANCED
SCIENCE NEWS**

www.advancedsciencenews.com

**ADVANCED
ELECTRONIC
MATERIALS**

www.advelectronicmat.de

X-ray diffraction (XRD) measurements spectrum for structural analysis of the deposited thin film. The prominent and well indexed sharp peaks at 15.12° and 30.47° with indices (101), (202) confirm higher crystallinity of orthorhombic structure of the $CsPbBr_3$ film. Two additional diffraction peaks at 12.10° and 48.02° marked with black dots, were assigned to another phase of perovskite represented by $CsPb_2Br_5$. The $CsPb_2Br_5$ phase possibly grew during the synthesis of $CsPbBr_3$ films by the low-temperature synthesis techniques.[24] It is clear from the weak diffraction peaks of XRD spectrum that $CsPb_2Br_5$ is present in very small amounts. Moreover, it was reported that the $CsPb_2Br_5$ possesses similar behavior to $CsPbBr_3$ and a very small amount of $CsPb_2Br_5$ did not show any significant effect on memory behaviors.[25]

The cross-sectional scanning electron microscope (SEM) image of the device and the surface morphology of the $CsPbBr_3$ thin film are shown in Figure 1c,d, respectively. The surface morphology image shows the $CsPbBr_3$ large size crystals (micro- and nanosizes) arranged densely over the whole surface of the substrate without any pinholes and nonhomogeneity. The crystallization process was very fast and the size of crystals is much larger than other hybrid organic–inorganic perovskites, due to the interaction between these materials and p-halogen.[26,27] Figure 1d represents the cross-sectional SEM image of $Au/CsPbBr_3/ITO/glass$ device structure. The atomic force microscope (AFM) analysis was performed to further confirm the smoothness and denseness of the as-prepared $CsPbBr_3$ films. The AFM topography image at 310 nm scale of $CsPbBr_3$ thin films is shown in Figure 1e, which showed a highly dense and compact film of $CsPbBr_3$ perovskites with the

calculated roughness (Ra) value of 14.2 nm. This also confirms that our two-step spin coating fabrication method can be used for the fabrication of improved surface morphology of $CsPbBr_3$ perovskites thin films.

The current–voltage curve for $Au/CsPbBr_3/ITO/Glass$ memory devices, as well as the electroforming process are plotted in **Figure 2**a and the inset. The electroforming mechanism leads to a controlled soft-breakdown in resistive behavior of the deposited material, which initiates the formation of localized conducting filaments. As a result of the electroforming and the conductive filament formation, the HRS/Off state transits to the LRS/On state. A forward voltage sweep is applied to reach the highest attainable current, followed by a reverse sweep to regain the initial state, which indicates that the device has been successfully electroformed. The $Au/CsPbBr_3/ITO/glass$ memory device showed typical bipolar switching behaviors. Switching mechanism has been observed in positive voltage direction. We applied bias voltage to the top Au electrode, and the bottom ITO electrode was grounded. As the increasing of the voltage bias from 0 to −3 V, the resistance state of device transformed from high resistance state (HRS) to low resistance state (LRS), which was called the switching process. During switching process the current suddenly increases from −0.20 V (called it as set voltage) and this process is termed as the "programming/writing" process (Figure 2a). In contrast, on the positive applied voltage biasing 0 → +3 V, device transforms from its LRS to HRS keeping compliance current 1 mA to avoid the breakdown of the memory device. In this process, the current suddenly dropped from 1.7 V (called it the reset voltage). Switching from LRS to HRS is commonly called the "erasing"
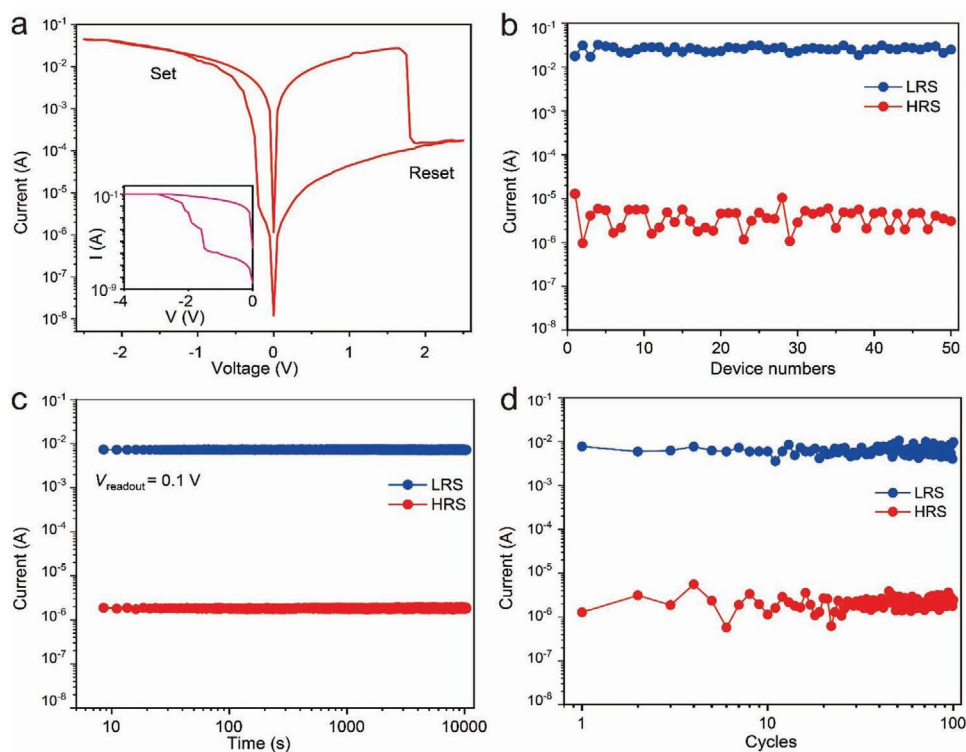

Figure 2. a) Typical current-voltage characteristics of $CsPbBr_3$ memory devices (inset: the plot of the electroforming process). b) Reproducibility for 50 devices showing almost stable LRS and HRS currents. c) Retention for 10^4 s without any significant change. d) The stability performance for 100 cycles.

Table 1. Brief summary of results reported on CsPbBr$_3$ based memory devices.

Structure	Set/reset voltage [V]	ON/OFF current ratio	Data retention [s]	Deposition method	Endurance Cycles	Ref.
Au/CsPbBr$_3$/FTO	1.5/−1.2	10^3	3×10^3	Spin coating	100	[28]
Pt/CsPbBr$_3$/Cu$_2$O/FTO	1.6/−1.5	$>10^3$		Spray coating	300	[29]
Au/Cs$_4$PbBr$_6$/PEDOT: PSS/Pt	0.6/−0.2	100	–	Spin coating	1000	[30]
Al/CsPbBr$_3$/PEDOT: PSS/ITO/PET	−0.6/1.7	10^2	–	Spin coating	50	[13]
Au/PMMA/PMMA: CsPbBr$_3$/PMMA/ ITO	1.4/−0.7	100	4000	Spin coating	40	[31]
Ag/CsPbBr$_3$/Pt	−0.5/0.6	$\approx 10^4$	$>5 \times 10^4$	Spin coating	–	[32]
Ag/PMMA/CsPbBr$_3$/PMMA/PET/ITO	2.3/−2.7	$\approx 10^5$	4×10^5	Spin coating	5000	[16]
Au/CsPbBr$_3$/ITO	−0.20/1.7	10^4	10^4	Two-step spin coating	100	This work

Note: FTO: fluorine-doped tin oxide; Cu$_2$O: cuprous oxide; PEDOT:PSS: poly(3,4-dihydrothieno-1,4-dioxin): poly(styrene sulfonate); PET: polyethylene terephthalate; PMMA: polymethylmethacrylate; Pt: platinum electrodes; Al: aluminum electrodes; Ag: silver electrodes.

process. The retention, as well as endurance properties, were examined at a bias voltage of 0.1 V, which is called the reading voltage. The devices exhibited excellent retention and reproducibility with almost no fluctuation even after repeated cycles, and for 50 devices, represented excellent reliability and stability. The brief analysis shows the device uniformity for multiple memory cells (Figure 2b).

The currents at On and Off states were ranging from 5.3×10^{-2} to 6.13×10^{-2} A and 2.59×10^{-6} to 2.99×10^{-6} A. Average set and reset voltages values were in the range of -0.20 ± 0.08 and 1.7 ± 0.37 V, respectively (Figure 2c). CsPbBr$_3$-based RRAM exhibits constant memory retention without any noticeable change for 10^4 s and 100 sweeping cycles, indicating competitive stability performance (Figure 2d). Complete resistive switching properties including set/reset voltages, retention process, ratio of On/Off current, retention, and processing method of previously reported perovskite RRAM were listed in **Table 1**. Comparing the previously reported RRAM results with our work, it indicates that our fabricated devices showed better bipolar resistive switching responses, consisting of the maximum On/Off current ratio, minimum Set/Reset voltages, long retention, stable cycling endurance performance, which are essential properties to the CsPbBr$_3$ thin films based memory devices.[33]

The comparison of current–voltage (I–V) characteristics with different fabricating methods for the CsPbBr$_3$ thin films was shown in **Figure 3**, including the two-step spin coating method (this work), the dipping after spin coating method and the dipping only method. The current–voltage curves indicated that the device fabricated by our two-step spin coating method (Figure 3a) is much stable and responds to lower set/reset voltage, compared to the devices fabricated by the other two methods (Figure 3b,c). The set and reset voltages of the memory devices with the three fabricating methods were summarized in Figure 3d. The two-step spin coating method exhibits a quite lower set voltage of −0.20 V, and a reset voltage of 1.86 V. The set/reset voltages were −1.85 V/2.0 V, and −0.95 V/1.95 V for the dipping after spin coating method and the dipping only method, respectively. The On/Off current ratio for the three processes were 10^4, 10^4, and 10^2, respectively. Set/reset values from the I–V curves revealed that the device fabricated with the two-step spin coating method in this work responds to the minimum power operating voltages, benefitting from the better

film morphology and smoother surface roughness of the as-prepared CsPbBr$_3$ films, which make the devices more energy efficient and cost effective.

The conductive filaments (CFs) model was used to explain the bipolar resistive switching memory mechanism for the as-prepared Au/CsPbBr$_3$/ITO/Glass memory devices (**Figure 4**). The relocation of Br$^-$ ions and the alignment of Br$^-$ vacancies are the major influence for the resistive switching mechanism. In the initial state, some randomly distributed Br$^-$ vacancies for the initial switching process exist in the CsPbBr$_3$ layer, illustrated in Figure 4-i. Under the applied positive electric field, Br$^-$ ions migrate to the positive electrode direction, leaving the Br$^-$ vacancies behind. Once it reaches to an optimum electric field, the Br$^-$ vacancies line up in such an orientation to make the CFs connect both the bottom and the top electrode, which is called the completeness of the alignment of Br$^-$ vacancies filaments state in the set process (Figure 4-ii).[34] The formation of CFs inside the perovskite switching layer transforms the device to the "On" state (LRS), by showing a sharp increase of the current. Commonly, the CFs formation is highly stable and strong enough at room temperature to break by insufficient driving force available at room temperature. Some theoretical calculations by using density functional theory and full potential-linearized augmented plane wave (FP-LAPW) method were reported, showing the effect of vacancies and metal ions toward improved performance of storage devices. In contrast, when reverse the applied electric field (opposite to the formation direction), it may force the Br vacancies to recombine with Br$^-$ ions in this region. Consequentially, the reset process happens and the resistance state of device transforms to the "Off" state (HRS) by the dissolution of filamentary conductive path, due to the electric field and Joule heating effect (rupture of filaments, Figure 4-iii). The resistive switching memory phenomenon is driven by the formation and the dissolution of Br$^-$ vacancy based CFs in the CsPbBr$_3$ layer of the Au/CsPbBr$_3$/ITO/ glass memory devices.[35]

To further analyze the carrier transport and understand the conduction mechanism of the CsPbBr$_3$ based memory device, the log I–log V curves were plotted and fitted for the set and reset process. **Figure 5**a,b shows the fitting plots of the I–V curves for the CsPbBr$_3$ memory cells in a logarithmic scale. The fitted data indicate that the conduction mechanism of LRS completely dominates, due to the Ohmic behavior of the device
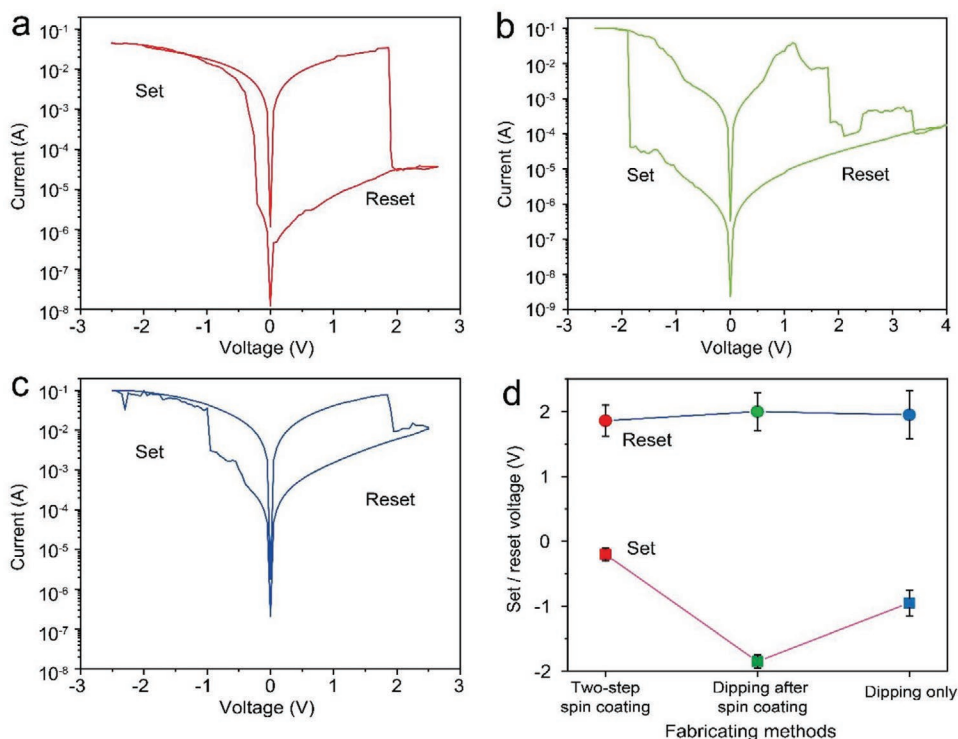
Figure 3. The current-voltage curves for different fabricating methods for the CsPbBr$_3$ thin films of the memory devices, by a) the two-step spin coating method, b) the dipping after spin coating method, and c) the dipping only method, respectively. d) Comparison of the set and reset voltages with the three fabricating methods.

at low bias voltage region (0–1.45 V) with the slope of 0.95 (close to 1, $I \propto V$), which can be attributed to the formation of the conductive filaments in CsPbBr$_3$ thin film layer. On the other hand, the space charge limited current (SCLC) phenomenon is used to explain the conduction mechanism in HRS. Due to the SCLC phenomenon, the current will dramatically increase when the voltage reaches to a certain level, according to the Child's square law ($I \sim V^2$). The voltage at which the transition from the trap-unfilled to the trap-filled region occurs is called threshold voltage (Figure 5a). This transition from the

Ohmic region to the Child's square region corresponds to the transition from the trap-unfilled to the trap-filled region of SCLC.[36,37]

Another prominent feature of this device is the excellent transient behavior. Novel electronic devices that can disappear partially or completely, either physically or functionally under some external stimuli are called transient electronics. Recently, several transient electronic devices were reported.[38] The significance of using transient materials for environment-friendly degradable sensors, biomedical implants, hardware-secured

Figure 4. Illustration of the conductive filament formation and resistive switching mechanism of the as-prepared memory device.
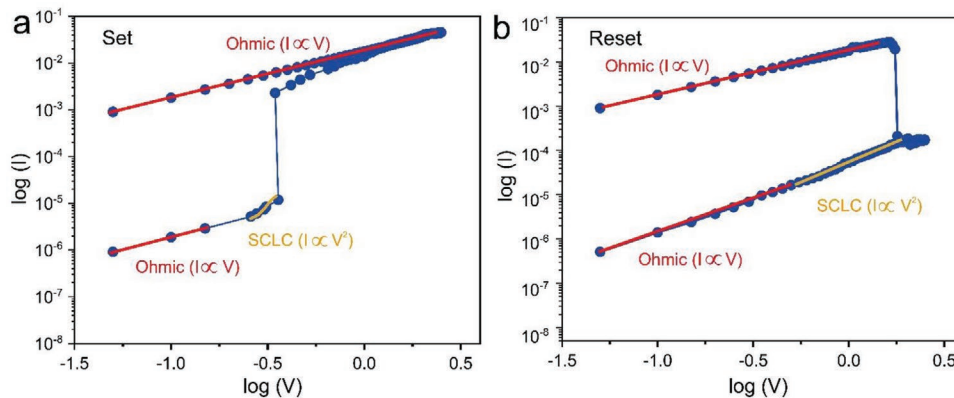
Figure 5. Schematic analysis for memory formation in Au/CsPbBr$_3$/ITO/Glass memory devices logarithmic plots of voltage and current with fitted conduction mechanism during a) negative direct current applied voltage (the set process) and b) positive direct current applied sweeps (the reset process).

digital systems, green electronics, and smart intelligence applications can never be denied. However, the degradation process normally requires quite a long time (up to several hours) in water, according to the reported works on the water-soluble transient ReRAM memory devices based on zinc oxide, magnesium oxide, egg albumen and fibroin substrate-based Au/magnesium (Mg)/fibroin/Mg devices.[39,40] In this work, we achieved much faster transient behavior of the CsPbBr$_3$ thin film based memory devices in deionized (DI) water at room temperature. The yellow perovskite film dissolved quickly after dipping in DI water and fully vanished within 60 s. The electrical characteristics including the current-voltage measurements, ultraviolet (UV) analysis and PL spectra for transient memory devices were shown in **Figure 6**a–c, respectively. Figure 6a reveals that after immersing the devices into the DI water, the device quickly loss its resistive switching function, without any noticeable memory responses. The UV spectrum of the original samples at room temperature shows a strong absorption peak at 500 nm. In contrast, after immersing in DI water for 60 s, the UV spectra showed rarely observable absorption peak of the CsPbBr$_3$ thin film (Figure 6b). The PL spectra in Figure 6c shows an intense peak at 517 nm before immersing, and barely noticeable peak after immersing in DI water for 60 s, which further proves the complete loss of the optical properties of CsPbBr$_3$ films by immersion in DI water. For a complete transient and self-destructive memory device, a dissolvable or degradable metal electrode can be used. These results reveal the promising application of the CsPbBr$_3$ material for transient memory devices, secured data storage and implantable electronics.

3. Conclusions

We have successfully demonstrated reproducible all-inorganic CsPbBr$_3$ based RRAM by solution processable method at ambient conditions. Highly dense CsPbBr$_3$ films with high crystallinity and without any pinholes were deposited on well cleaned ITO substrates. The bipolar resistive switching characteristics of the CsPbBr$_3$ thin film include high on/off ratio (≈10000), long-term data retention (over 10000 s) and low energy consumption with a small set voltage of 0.25V. Conductive filament model is employed to elucidate the resistive switching mechanism in the memory device made of Au/CsPbBr$_3$/ITO/ glass. Furthermore, the CsPbBr$_3$ layer can be dispersed in water within 60 s, showing an exceptional transient response. These results reveal that our approach to preparing high quality CsPbBr$_3$ films with low cost and high stability is promising for fabricating the next generation data storage devices.

4. Experimental Section

Chemicals and Reagents: The chemicals used in this work included cesium bromide (CsBr, 99.99%), lead bromide (PbBr$_2$, 98%), anhydrous methanol (CH$_3$OH, 99.8%), and *N,N*-dimethylformamide (DMF, 99.8%), and were used directly as received from Sigma-Aldrich (Germany).

Materials Preparation: 30 mg of CsBr and 367 mg of PbBr$_2$ were completely dissolved in 2 mL CH$_3$OH and 1 mL DMF, respectively. CsBr/CH$_3$OH solution was stirred at 60 °C for 15 min, while PbBr$_2$/ DMF solution was stirred constantly at 75 °C for 5 h to form completely transparent solutions. PbBr$_2$/DMF solution was filtered by 0.22 μm polytetrafluoroethylene (PTFE) filters before deposition.
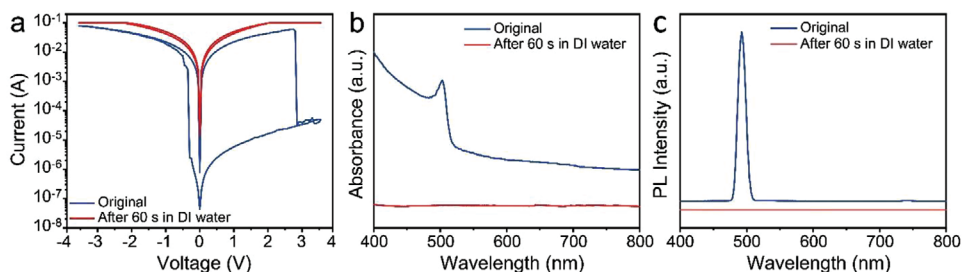

Figure 6. The transient behavior of CsPbBr$_3$ perovskite films, before and after 60 s dipping in DI water at room temperature. a) The current–voltage response of the devices. b) Ultraviolet absorbance spectra. c) Photoluminescence spectra.

Devices Fabrication: The fabrication of memory devices consists of three main steps, which include, the substrates treatment, the deposition of the perovskite layer and the deposition of the top gold electrode. In previous reports, the $PbBr_2$ was spin coated and the substrates were dipped in CsBr solution to form $CsPbBr_3$.[41,42] However, the dipping process usually causes nonuniform distribution and irregular grain sizes. In this work, $PbBr_2$ and CsBr were successfully spin-coated, separately to form the $CsPbBr_3$ perovskite layer, with satisfactory surface morphology and reduced defects. Starting with 20 min ultrasonically cleaning ITO substrates (150 nm) in DI water, acetone, and isopropanol, respectively. After that, the ITO substrates were dried under nitrogen (N_2). Ultraviolet-ozone (UVO) irradiation treatment was applied to improve the adhesion between the perovskite layer and the ITO layer. Then the $CsPbBr_3$ layer was fabricated. Initially, the transparent $PbBr_2$/DMF solution was filtered and deposited at 3000 rpm/40 s and placed on a hotplate at 75 °C for 20 min. Next, the $CsBr$/CH_3OH solution was spin coated at 2000 rpm/30 s and then dried at 80 °C for 30 min. The as-prepared samples were placed in the vacuum drying oven at 75 °C for 24 h. Finally, the top Au electrode of 80 nm thickness was deposited on the $CsPbBr_3$ layer through a shadow mask via vacuum evaporation.

Characterizations: XRD was used for structural analysis of the $CsPbBr_3$ perovskite samples (XRD-6100, SHIMADZU, Japan). Surface morphology and the cross-sectional view of the perovskite layer were observed by using the (SEM, Jeol JSM-7800F, Japan). Complete electrical characteristic analysis of the memory cells was carried out by a semiconductor parameter analyzer (Keithley 4200, Keithley Instruments Inc., USA) at room temperature. Room temperature absorption spectra in the range of 400–800 nm were recorded by an ultraviolet–visible spectrophotometer (UV–vis, PerkinElmer Lambda 950, USA). Photoluminescence spectra were measured by a fluorescence spectrophotometer (FL, FL-70000, PerkinElmer Elmer, USA). The AFM (Asylum Research MFP-3D, USA) analysis was done for the surface morphology characterization.

Acknowledgements

Conflict of Interest

The authors declare no conflict of interest.

Data Availability Statement

The data that support the findings of this study are available from the corresponding author upon reasonable request.

Keywords

[1] M. M. Waldrop, *Nature* **2016**, *530*, 144.
[2] M. M. Shulaker, G. Hills, R. S. Park, R. T. Howe, K. Saraswat, H. P. Wong, S. Mitra, *Nature* **2017**, *547*, 74.
[3] H. W. Huang, C. F. Kang, F. I. Lai, J. H. He, S. J. Lin, Y. L. Chueh, *Nanoscale Res. Lett.* **2013**, *8*, 483.
[4] H. Algadi, C. Mahata, T. Alsuwian, M. Ismail, D. Kwon, S. Kim, *Mater. Lett.* **2021**, *298*, 130011.
[5] Z. Lv, X. Xing, S. Huang, Y. Wang, Z. Chen, Y. Gong, Y. Zhou, S.-T. Han, *Matter* **2021**, *4*, 1702.
[6] J. Chen, J. Wang, X. Xu, J. Li, J. Song, S. Lan, S. Liu, B. Cai, B. Han, J. T. Precht, *Nat. Photonics* **2021**, *15*, 238.
[7] Z. Li, F. Sun, Z. Zheng, J. Chen, A. V. Davydov, S. Deng, H. Zhang, H. Chen, F. Liu, *Nano Lett.* **2021**, *21*, 1822.
[8] L. Jin, Y. Zhang, M. Cao, Y. Yu, Z. Chen, Y. Li, Z. Zhong, X. Hua, L. Xu, C. Cai, *Nanotechnology* **2021**, *32*, 235203.
[9] K. Lin, J. Xing, L. N. Quan, F. P. G. de Arquer, X. Gong, J. Lu, L. Xie, W. Zhao, D. Zhang, C. Yan, *Nature* **2018**, *562*, 245.
[10] Y. Cheng, S. Da Ling, Y. Geng, Y. Wang, J. Xu, *Nanoscale Adv.* **2021**, *3*, 2180.
[11] H. Algadi, A. Umar, H. Albargi, T. Alsuwian, S. Baskoutas, *Crystals* **2021**, *11*, 717.
[12] W. Hu, L. Zou, X. Chen, N. Qin, S. Li, D. Bao, *ACS Appl. Mater. Interfaces* **2014**, *6*, 5012.
[13] J. Lee, W. D. Lu, *Adv. Mater.* **2018**, *30*, 1702770.
[14] D. Liu, Q. Lin, Z. Zang, M. Wang, P. Wangyang, X. Tang, M. Zhou, W. Hu, *ACS Appl. Mater. Interfaces* **2017**, *9*, 6171.
[15] R. Wang, H. Li, L. Zhang, Y.-J. Zeng, Z. Lv, J.-Q. Yang, J.-Y. Mao, Z. Wang, Y. Zhou, S.-T. Han, *J. Mater. Chem. C* **2019**, *7*, 10203.
[16] Y. Wang, Z. Lv, Q. Liao, H. Shan, J. Chen, Y. Zhou, L. Zhou, X. Chen, V. A. Roy, Z. Wang, Z. Xu, Y.-J. Zeng, S.-T. Han, *Adv. Mater.* **2018**, *30*, 1800327.
[17] J. Silva, C. A. Marques, J. A. Moreira, O. Conde, *J. Mater. Chem. C* **2017**, *5*, 10353.
[18] C. Gu, J. S. Lee, *ACS Nano* **2016**, *10*, 5413.
[19] Z. Li, L. Kong, S. Huang, L. Li, *Angew. Chem., Int. Ed.* **2017**, *56*, 8134.
[20] Q. Zhou, J. Duan, J. Du, Q. Guo, Q. Zhang, X. Yang, Y. Duan, Q. Tang, *Adv. Sci.* **2021**, *8*, 2101418.
[21] J. Liu, K. Chen, S. A. Khan, B. Shabbir, Y. Zhang, Q. Khan, Q. Bao, *Nanotechnology* **2020**, *31*, 152002.
[22] X. Chang, W. Li, L. Zhu, H. Liu, H. Geng, S. Xiang, J. Liu, H. Chen, *ACS Appl. Mater. Interfaces* **2016**, *8*, 33649.
[23] J. Zheng, C. Luo, B. Shabbir, C. Wang, W. Mao, Y. Zhang, Y. Huang, Y. Dong, J. J. Jasieniak, C. Pan, Q. Bao, *Nanoscale* **2019**, *11*, 8020.
[24] K. H. Wang, L. Wu, L. Li, H. B. Yao, H. S. Qian, S. H. Yu, *Angew. Chem., Int. Ed.* **2016**, *55*, 8328.
[25] X. Zhang, B. Xu, J. Zhang, Y. Gao, Y. Zheng, K. Wang, X. W. Sun, *Adv. Funct. Mater.* **2016**, *26*, 4595.
[26] O. Khyzhun, P. Fochuk, I. Kityk, M. Piasecki, S. Levkovets, A. Fedorchuk, O. Parasyuk, *Mater. Chem. Phys.* **2016**, *172*, 165.
[27] R.-H. Shen, S.-H. Yang, P.-Y. Lin, *ACS Appl. Electron. Mater.* **2020**, *2*, 1619.
[28] H. Cai, G. Ma, Y. He, L. Lu, J. Zhang, H. Wang, *Ceram. Int.* **2019**, *45*, 1150.
[29] H. Liu, Y. Wu, Y. Hu, *Ceram. Int.* **2017**, *43*, 7020.
[30] H. Cai, M. Lao, J. Xu, Y. Chen, C. Zhong, S. Lu, A. Hao, R. Chen, *Ceram. Int.* **2019**, *45*, 5724.
[31] X. Zhang, H. Yang, Z. Jiang, Y. Zhang, S. Wu, H. Pan, N. Khisro, X. Chen, *J. Phys. D: Appl. Phys.* **2019**, *52*, 125103.
[32] Y. Zhu, P. Cheng, J. Shi, H. Wang, Y. Liu, R. Xiong, H. Ma, H. Ma, *Adv. Electron. Mater.* **2019**, *6*, 1900754.
[33] S. J. Song, J. Y. Seok, J. H. Yoon, K. M. Kim, G. H. Kim, M. H. Lee, C. S. Hwang, *Sci. Rep.* **2013**, *3*, 3443.
[34] T. Alsuwian, F. Kousar, U. Rasheed, M. Imran, F. Hussain, R. A. Khalil, H. Algadi, N. Batool, E. A. Khera, S. Kiran, *Chaos, Solitons Fractals* **2021**, *150*, 111111.

**ADVANCED
SCIENCE NEWS**

www.advancedsciencenews.com

**ADVANCED
ELECTRONIC
MATERIALS**

www.advelectronicmat.de

[35] E. A. Khera, H. Ullah, M. Imran, R. A. Khalil, F. Hussain, H. Algadi, *Adv. Theory Simul.* **2021**, *4*, 2100011.

[36] C.-H. Huang, W.-C. Chang, J.-S. Huang, S.-M. Lin, Y.-L. Chueh, *Nanoscale* **2017**, *9*, 6920.

[37] M. Ismail, U. Chand, C. Mahata, J. Nebhen, S. Kim, *J. Mater. Sci. Technol.* **2022**, *96*, 94.

[38] Q. Xue, T. Hang, Z. Gong, L. Chen, J. Liang, Y. Sun, D. Lu, X. Zhang, C. C. Chen, M. Li, *Adv. Electron. Mater.* **2021**, *7*, 2100322.

[39] M. M. Rehman, H. M. M. ur Rehman, W. Y. Kim, S. S. H. Sherazi, M. W. Rao, M. Khan, Z. Muhammad, *ACS Appl. Electron. Mater.* **2021**, *3*, 2832.

[40] F. Song, H. Wang, J. Sun, H. Gao, S. Wu, M. Yang, X. Ma, Y. Hao, *IEEE Electron Device Lett.* **2017**, *39*, 31.

[41] Q. Lin, W. Hu, Z. Zang, M. Zhou, J. Du, M. Wang, S. Han, X. Tang, *Adv. Electron. Mater.* **2018**, *4*, 1700596.

[42] Y. Li, L. Ji, R. Liu, C. Zhang, C. H. Mak, X. Zou, H.-H. Shen, S.-Y. Leu, H.-Y. Hsu, *J. Mater. Chem. A* **2018**, *6*, 12842.

2101412 (8 of 8)